Defect-engineered silica with temperature-responsive conversion of yellow and blue afterglow

Ying Sun[a,+], Fengyuan Ma[a,+], Xinke Wang[a,+], Zexi Li[b], Yanmei Yang[a], Ran Feng[a], Fei Zhang[a], Shenghong Yang[c], Ke Tang[d,*], Jian Liu[a,*]

[a]School of Chemical Engineering, College of Chemistry and Materials, State–Province Joint Engineering Laboratory of Zeolite Membrane Materials, Jiangxi Normal University, Nanchang, 330022, China.

[b]Guoye Shandong Bureau Group Geological Experiment Testing Technology Co., Ltd., Jinan, 250000, China.

[c]Shandong Provincial Key Laboratory of Molecular Engineering, School of Chemistry and Chemical Engineering, Qilu University of Technology (Shandong Academy of Sciences), Jinan, 250353, China.

[d]School of Chemistry and Chemical Engineering, Heze University, Heze, 274015, China.

[+]The authors contributed equally to this work.

***Corresponding Authors:**

Email: tangke@hezeu.edu.cn (K. Tang); jianliu18@jxnu.edu.cn (J. Liu)

1. Experimental Section

1.1 Chemicals

Tetraethyl orthosilicate (TEOS), $NH_3 \cdot H_2O$ (30 wt%), polyvinyl alcohol (PVA, MW130000), phenol, o-dihydroxybenzene (o-DHB), m-dihydroxybenzene (m-DHB), p-dihydroxybenzene (p-DHB), and trihydroxybenzene (THB), hydrofluoric acid, ethanol, methanol, ethylene glycol (EG), N,N-dimethylformamide (DMF), dimethyl sulfoxide (DMSO), acetonitrile, tetrahydrofuran (THF), dichloromethane (DCM), n-hexane, rhodamine 6G (Rh6G). All reagents were purchased from Aladdin, Shanghai, and used as received without further purification. Pure water was used during the experiment.

1.2 Measurements

Morphology and physical structure: Morphologies were detected by a JEM-2100 transmission electron microscope (TEM) and a SU8000 field-emission scanning electron microscope (SEM). X-ray powder diffraction (XRD) data were collected on a Bruker AXS D8-Advanced diffractometer with Cu Kα radiation (λ = 1.5418 Å).

Chemical composition: Fourier transform infrared (FT-IR) spectra were obtained on a Nicolet 6700 FT-IR spectrometer. X-ray photoelectron spectroscopy (XPS) analysis was tested on Thermo Scientific K-Alpha with Al Kα radiation. Contents of carbon and oxygen were analyzed on a carbon sulfur analyzer (CS2800) and oxygen-nitrogen-hydrogen analyzer (HORIBA EMGA-930), respectively. Approximately 200 mg of silica samples were used for test. Atomic ratios of O/Si and C/Si were then calculated based on the mass percentages (wt%).

Photophysical test: Steady-state photoluminescence spectra were measured on a photoluminescence spectrometer (Lengguang F97). Time-resolved decay spectra were recorded on a photoluminescence spectrometer (FLS1000, Edinburgh). The absolute quantum yield was measured using a photoluminescence spectrometer (C9920-02G, Hamamatsu) coupled with an integrating sphere. Electron spin resonance (ESR) spectra were recorded on a Bruker EMXPLUS spectrometer under UV on/off stimuli. Approximately 50 mg of silica samples were used for test. Thermoluminescence (TL) spectra were obtained by a cryostat controlled by a cooling–heating stage (THMS600E, Linkam Scientific Instruments), and excited by a 254 nm light-emitting diode with a 5 mW cm^{-2} excitation power density for 30 s. The emission was monitored in a temperature range between 30 ~ 300 °C. A filter-attached PMT (R928P, Hamamatsu Photon-ics), a multimeter (2400, Keithley) and a high-voltage power supply (HVC1800, Zolix) simultaneously monitored

the luminescence intensity. TL emission spectra were recorded at the same time by using a multichannel spectrometer (QE-Pro, Ocean Optics) with a rate of 1 °C s^{-1}.

1.3 Synthesis of Stöber SiO_2, phenols@SiO_2, and doped silica

Stöber SiO_2 and annealed SiO_2: Stöber SiO_2 particles were synthesized according to a modified Stöber method.[1] Typically, 1 mL of $NH_3 \cdot H_2O$ (30%) and 1 mL of TEOS were successively added into a mixture of ethanol (26 mL) and H_2O (5 mL). After being stirred at *r.t.* for 6 h, products were collected by centrifugation (7000 rpm, 3 min) and then washed with ethanol three times. The products were dried under vacuum at 100 °C for 6 h to remove residual solvents. Stöber SiO_2 were annealed at various temperatures for 4 h with a heating rate of 5 °C/min under N_2 (or air).

phenols@SiO_2 and annealed doped SiO_2: Phenols-loaded SiO_2 (phenols@SiO_2) were synthesized similar to the Stöber's method, except adding diverse phenols. Typically, phenols (0.5, 1, 3, 5, and 7 mmol), 5 mL of H_2O, 26 mL of ethanol, 1 mL of TEOS, and 1 mL of $NH_3 \cdot H_2O$ (30%) were mixed and stirred at *r.t.* for 4 h. The products were dried under vacuum at 100 °C for 6 h to remove residual solvents. Products were collected by centrifugation (7000 rpm, 3 min) and then washed with ethanol three times. Here, phenol, o-DHB, m-DHB, p-DHB, and THB were used as organic carbon sources, and the corresponding products were denoted as p@SiO_2, o-DHB@SiO_2, m-DHB@SiO_2, p-DHB@SiO_2, and THB@SiO_2, respectively. Typically, the phenols@SiO_2 were annealed at various temperatures for 4 h with a heating rate of 5 °C/min under N_2 (or air). The p@SiO_2 with n mmol of feeding phenol and annealing treatments at 600, 700, 800, 850, and 900 °C under N_2 were denoted as ***A-n***, ***B-n***, ***C-n***, ***D-n***, and ***E-n***, respectively. Moreover, p@SiO_2 with 5 mmol of feeding phenol and annealing at t °C under N_2 or air were also denoted as *p@SiO_2 (N_2-t)* or *p@SiO_2 (air-t)*, respectively.

1.4 Device and information encryption of doped silica

SiO_2/PVA films: PVA (0.5 g) was dissolved in 10 ml of H_2O at 60 °C. Then, 50 mg of ***D-0.5*** was added to the above PVA solution, sonicated and stirred to form a homogeneous suspension. Two millilitres of the suspension was added to a round dish mold and gently dried at *r.t.* to obtain SiO_2/PVA films.

SiO_2/PVA tablets: PVA powder (1 g) and ***D-0.5*** (50 mg) were mixed directly in a mortar, and then the powder mixture was pressed into tablets with a diameter of 2 cm.

Similarly, diverse small SiO_2/PVA tablets (diameter, 0.5 cm) were prepared and used as building blocks

to assemble special patterns for information encryption demonstration.

1.5 Fabrication of SiO_2-charged LED device

An LED device was fabricated using ***D-5*** as a photoluminescent resource. ***D-5*** were finely encased in Super Glue onto a prototype solid-state lighting unit comprising the commercial LED chips with λ_{max} = 380 nm (substrate: sapphire; epitaxial: GaN-based material; pad material: Au alloy; backside metal: Al). The device was operated at 4.3 V forward voltage and 350 mA forward current. The emission spectrum of this device was measured by a luminescence spectrometer.

1.6 Spatial-time-temperature-resolved anticounterfeiting application

Four types of doped silica, including *p@SiO$_2$(N_2-500)*, *p@SiO$_2$(N_2-600)*, *p@SiO$_2$(N_2-850)*, and *p@SiO$_2$(air-600)*, were used as examples to demonstrate the spatial-time-temperature-resolved anticounterfeiting application. PVA aqueous solutions (5 mg mL^{-1}) containing different types of doped silica (10 mg mL^{-1}) were prepared after sonication for 10 min separately as anticounterfeiting inks. With the aid of a mold featuring a butterfly pattern, the inks were sprayed selectively onto different areas of an Al foil. After drying thoroughly on a heating plate (353 K), a butterfly pattern integrated with different types of doped silica was fabricated. The encrypted pattern was placed on a heating plate at varying temperatures, and its photoluminescent properties were gathered under 365 nm or 254 nm on/off stimuli. Subsequently, a spatial-time-temperature-resolved anticounterfeiting application was demonstrated with the Al foam on a plate with a gradient temperature (-190 ~ 200 °C).

2. Calculation of energy gap, lifetime, and quantum yield

Generally, RISC process hardly occur at 77K, leading to significant suppression of delayed FL and allowing phosphorescence (PH) to dominate the afterglow emission.[2-4] As such, the energy gap (ΔE_{ST}) between the lowest triplet excited state (T_1) and the lowest singlet excited state (S_1) can be estimated based on the FL and afterglow spectra at 77 K. The FL spectrum of ***D-5*** at 77 K still showed multiple peaks, while the afterglow spectrum only reserved the **Y** band, with peaks above 500 nm (Figure 4h). Adjacent peaks observed at 381 and 534 nm were used to calculate ΔE_{ST} according to the equation $E = 1240/\lambda$, yielding $\Delta E_{ST} = E_S - E_T$ = 0.93 eV.[2-4] The ΔE_{ST} value is above the ideal values for efficiently producing DF (< 0.2 eV), which is hardly to facilitate efficient RISC processes for DF.[5,6]

Both FL and afterglow decay spectra were fitted with a bi-exponential function well, with an initially fast decay process followed by a slow decay. The average lifetime was calculated as $\tau_{avg} = \sum \alpha_i \tau_i^2 / \sum \alpha_i \tau_i$, where τ_{avg}, τ_i, and α_i are average lifetime, multiexponential lifetime, and the corresponding proportions, respectively.[7,8] There are two components of the lifetime that compose the lifetime of the FL and afterglow, as shown in Table S3. Using ***D-5*** as an example, components of 8.40 ns (17.56%) and 73.99 ns (82.44%) compose the lifetime of 493 nm of FL emission (*Ex.* 320 nm), while that of 0.79 s (3.87%) and 3.65 s (96.13%) compose the lifetime of 571 nm of afterglow emission (*Ex.* 320 nm). The corresponding τ_{avg} of FL and afterglow emission were calculated as 62.48 ns and 3.54 s, respectively. The absolute quantum yield (QY) was measured using an equation QY = $N_{emitted}/N_{absorbed}$, where $N_{emitted}$ and $N_{absorbed}$ represent the numbers of photons emitted and absorbed, respectively.[9]

3. Supplementary Figures

3.1 Preparation and characterization of doped silica

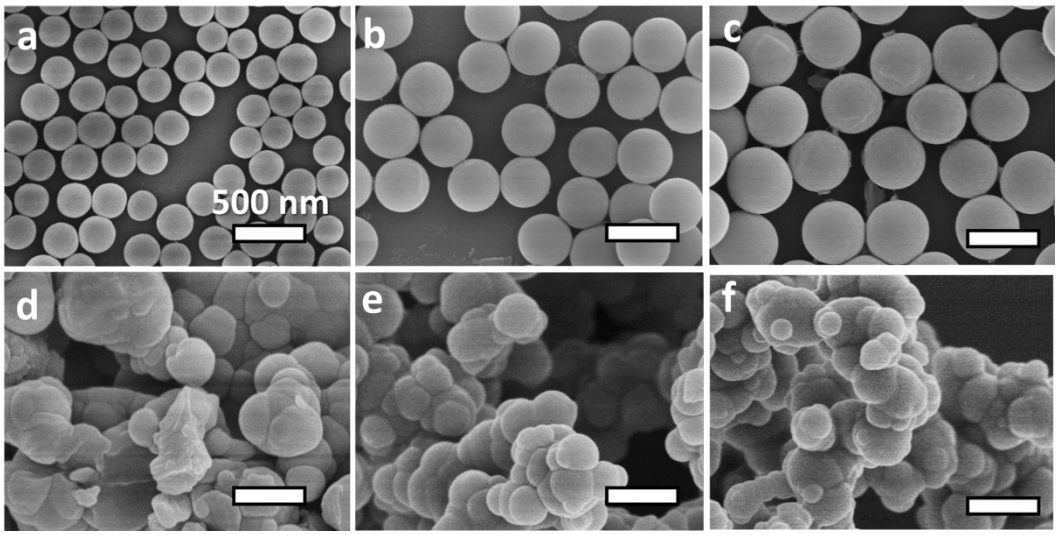

Fig. S1 SEM images of o-DHB@SiO_2 with (a-f) 0, 0.5, 1, 3, 5, and 7 mmol of feeding o-DHB. Scale bar is 500 nm.

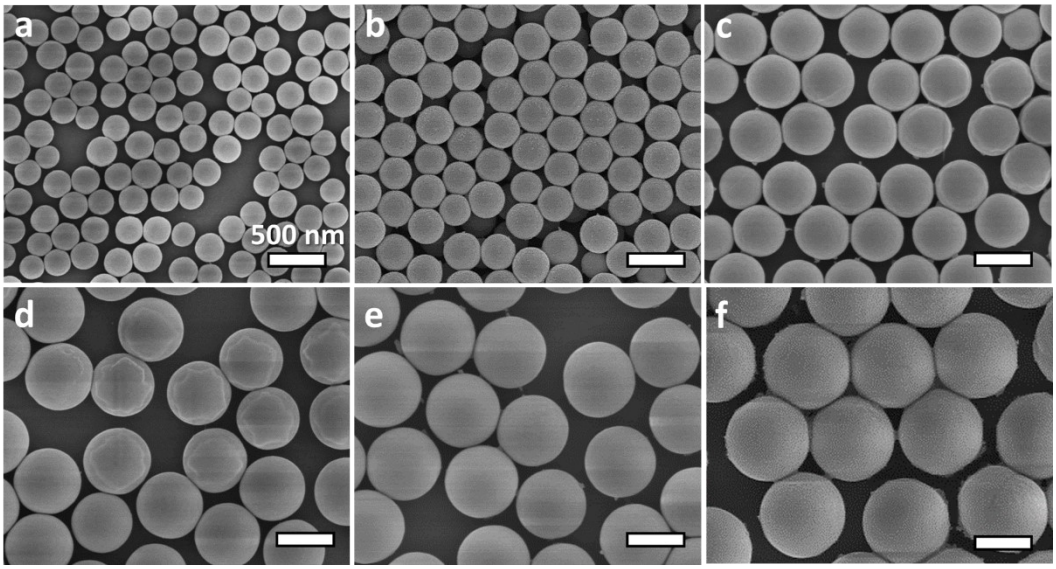

Fig. S2 SEM images of m-DHB@SiO_2 with (a-f) 0, 0.5, 1, 3, 5, and 7 mmol of feeding m-DHB. Scale bar is 500 nm.

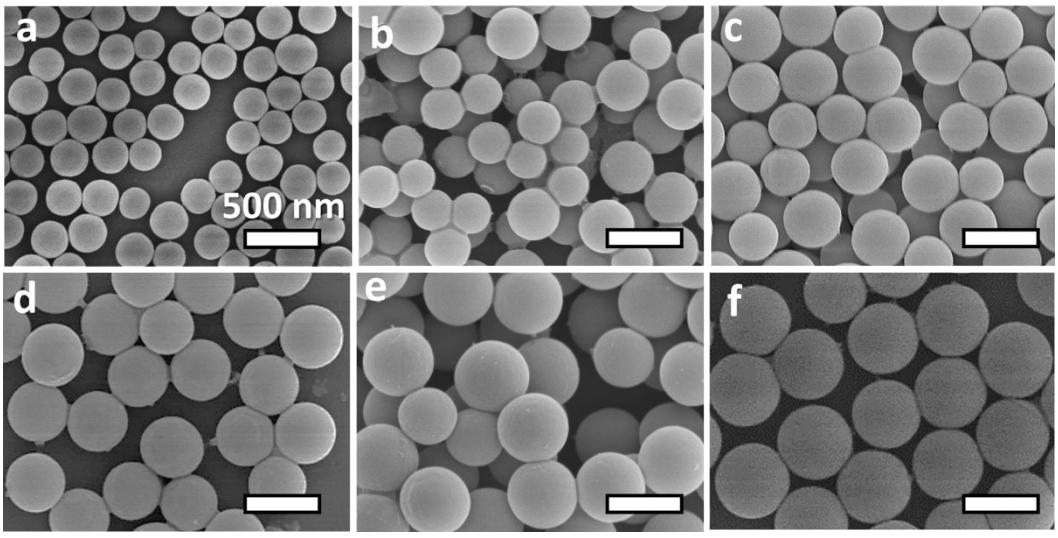

Fig. S3 SEM images of p-DHB@SiO_2 with (a-f) 0, 0.5, 1, 3, 5, and 7 mmol of feeding p-DHB. Scale bar is 500 nm.

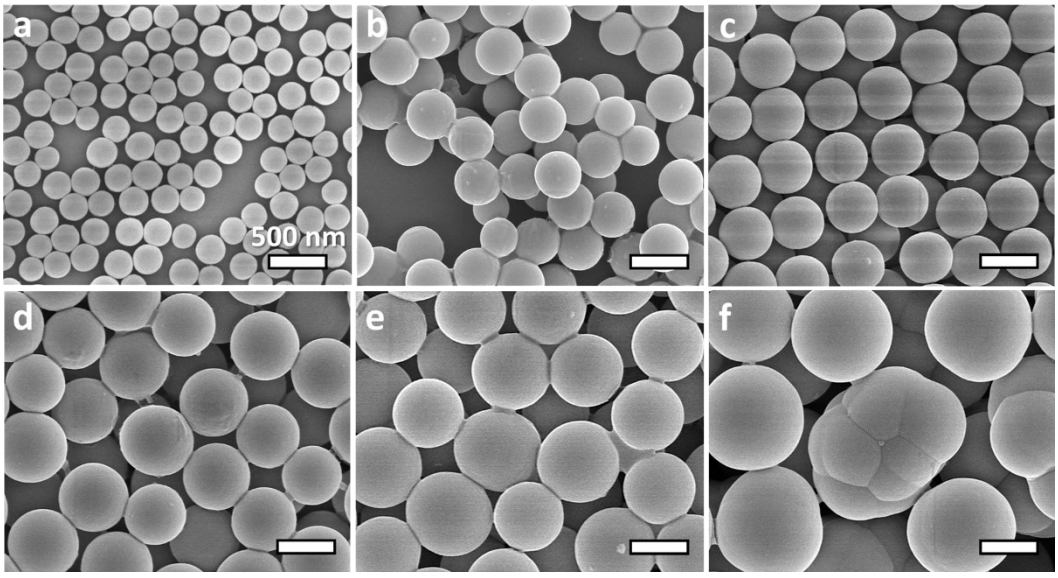

Fig. S4 SEM images of THB@SiO_2 with (a-f) 0, 0.5, 1, 3, 5, and 7 mmol of feeding THB. Scale bar is 500 nm.

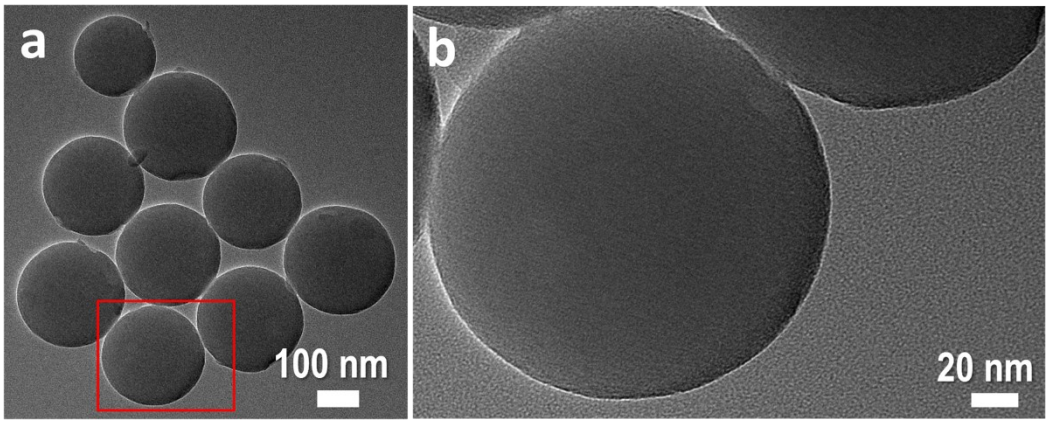

Fig. S5 TEM images of *SiO_2-A (850 °C)*. No nano-aggregates can be observed within the silica.

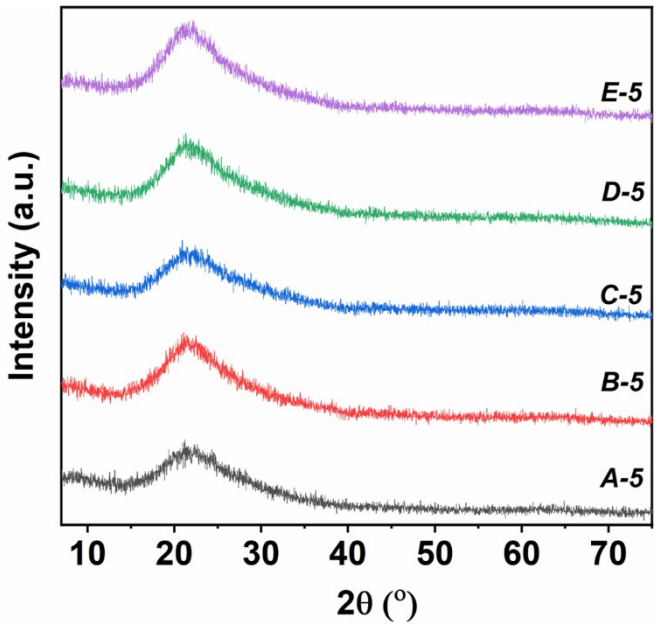

Fig. S6 XRD spectra of annealed silica.

3.2 Photophysical properties

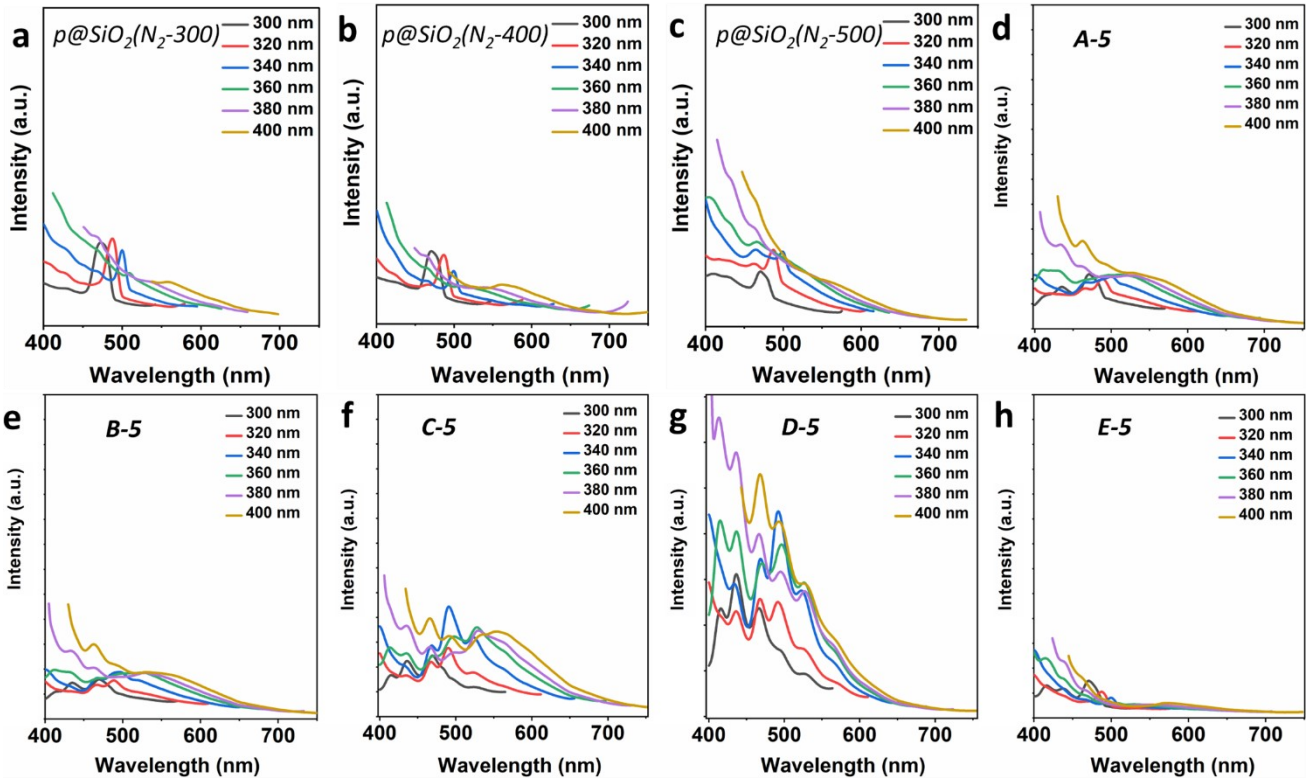

Fig. S7 Fluorescence spectra of various annealed p@SiO_2-5 (a~h, 300 ~ 900 °C) under different excitation wavelengths.

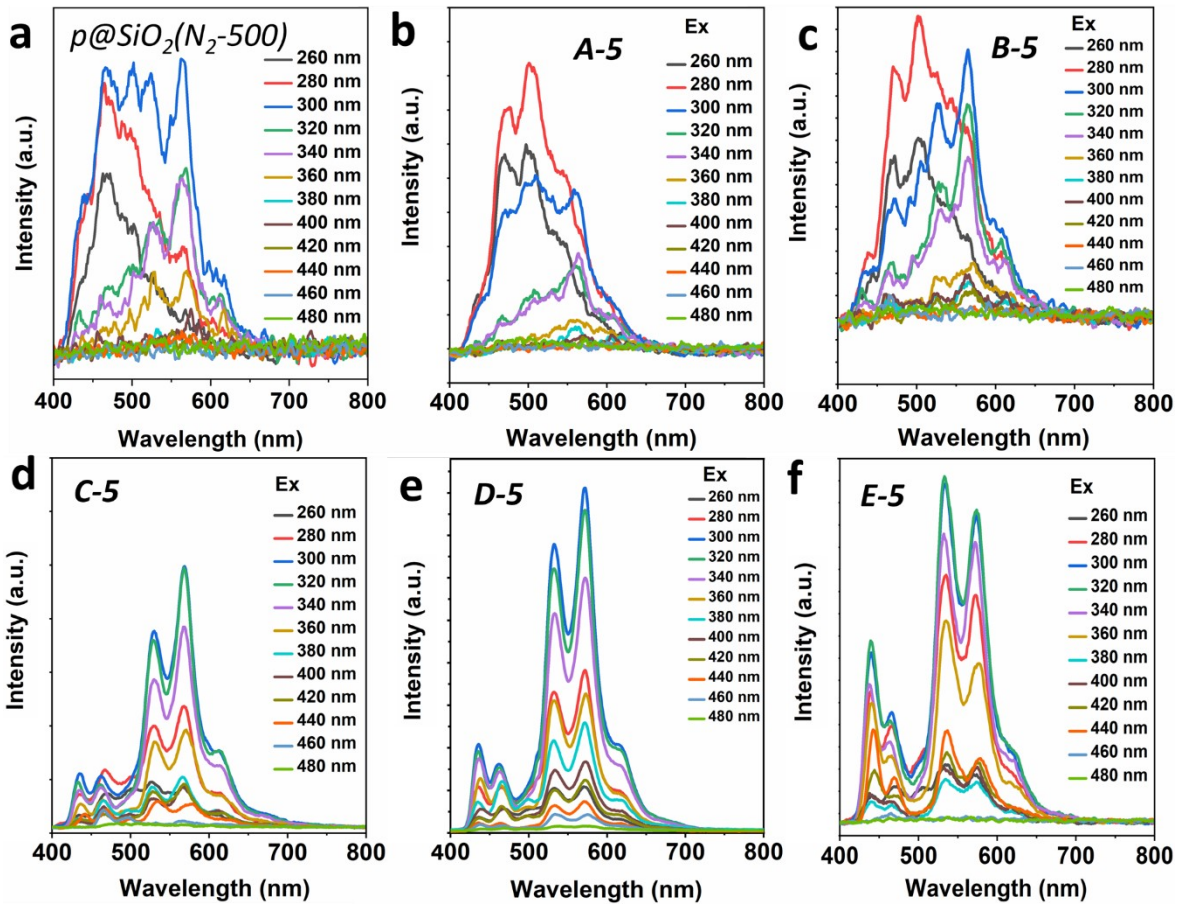

Fig. S8 Afterglow spectra of annealed p@SiO_2-5 under different excitation wavelengths.

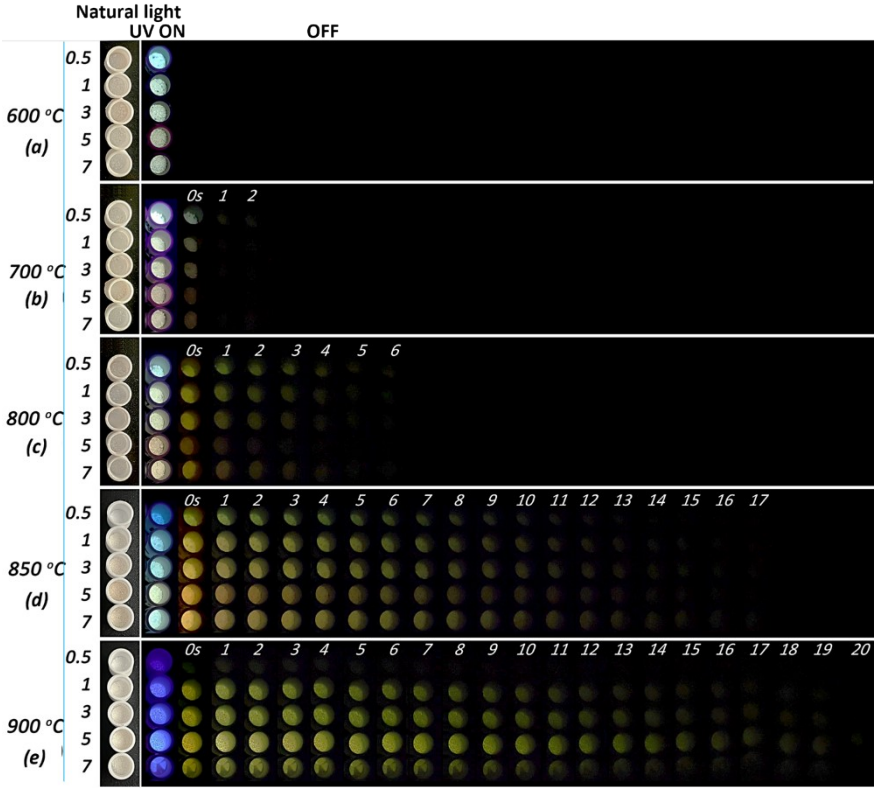

Fig. S9 Digital photos of various annealed THB@SiO_2 under natural light, 365 nm UV light on/off.

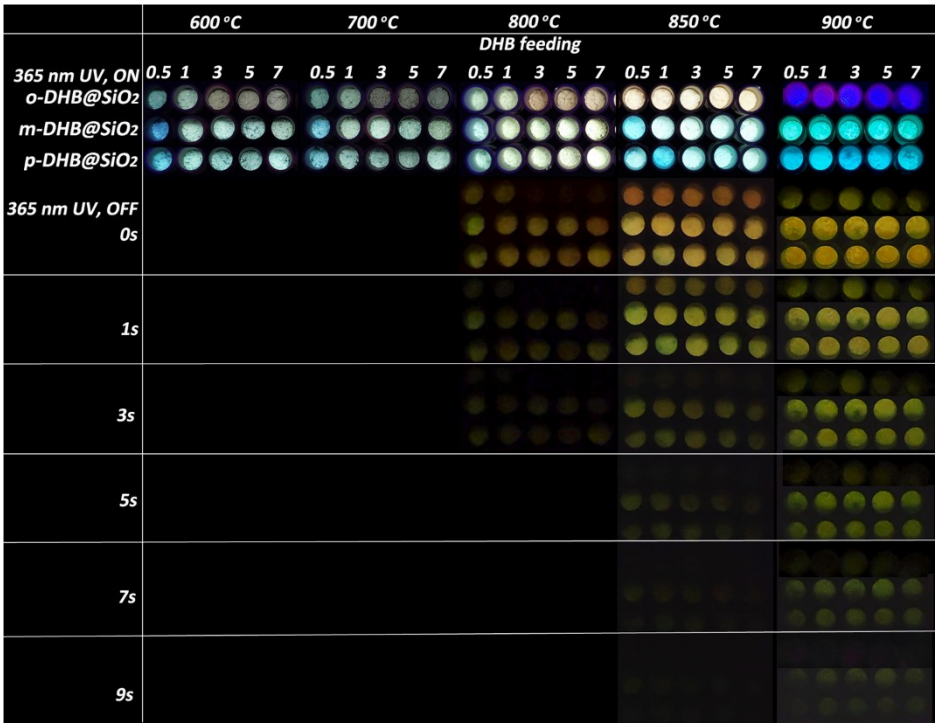

Fig. S10 Digital photos of various annealed phenols@SiO_2 (o-DHB@SiO_2, m-DHB@SiO_2, and p-DHB@SiO_2) under 365 nm UV light ON/OFF irradiation.

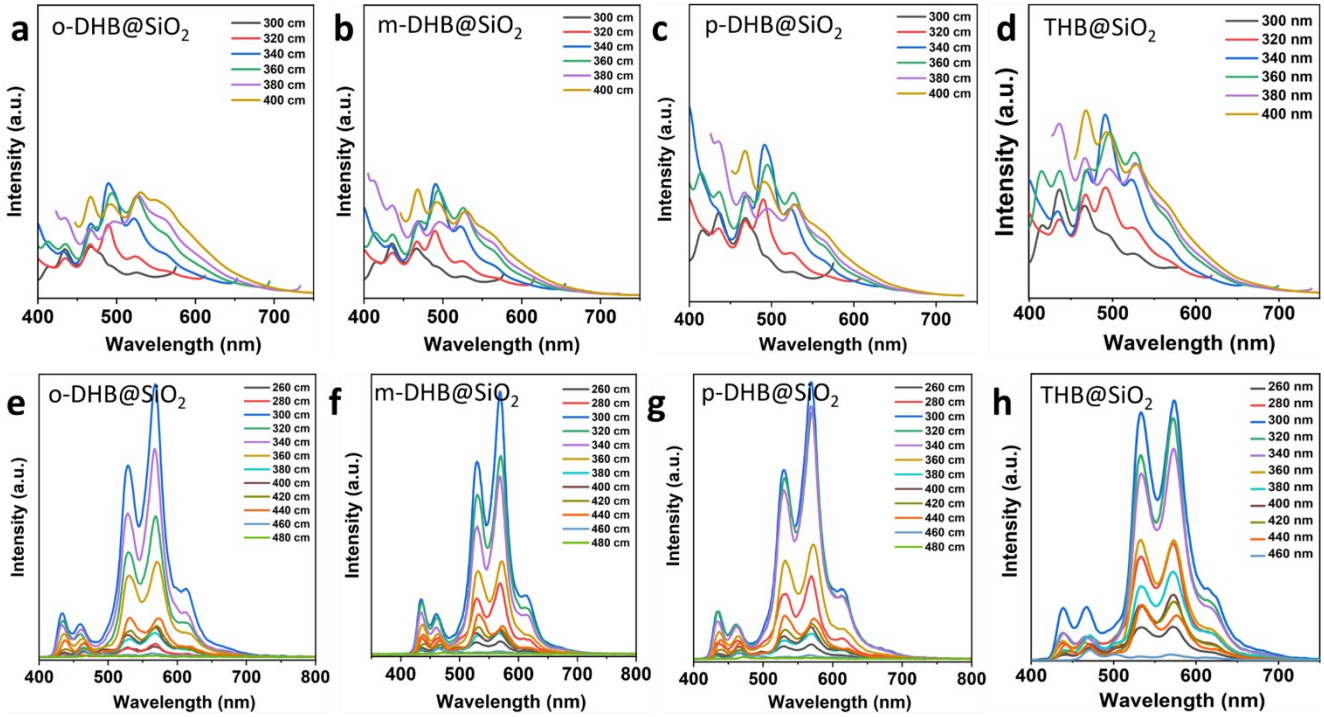

Fig. S11 (a-d) Fluorescence and (e-h) afterglow spectra of various annealed silica (850 °C) under different excitation wavelengths.

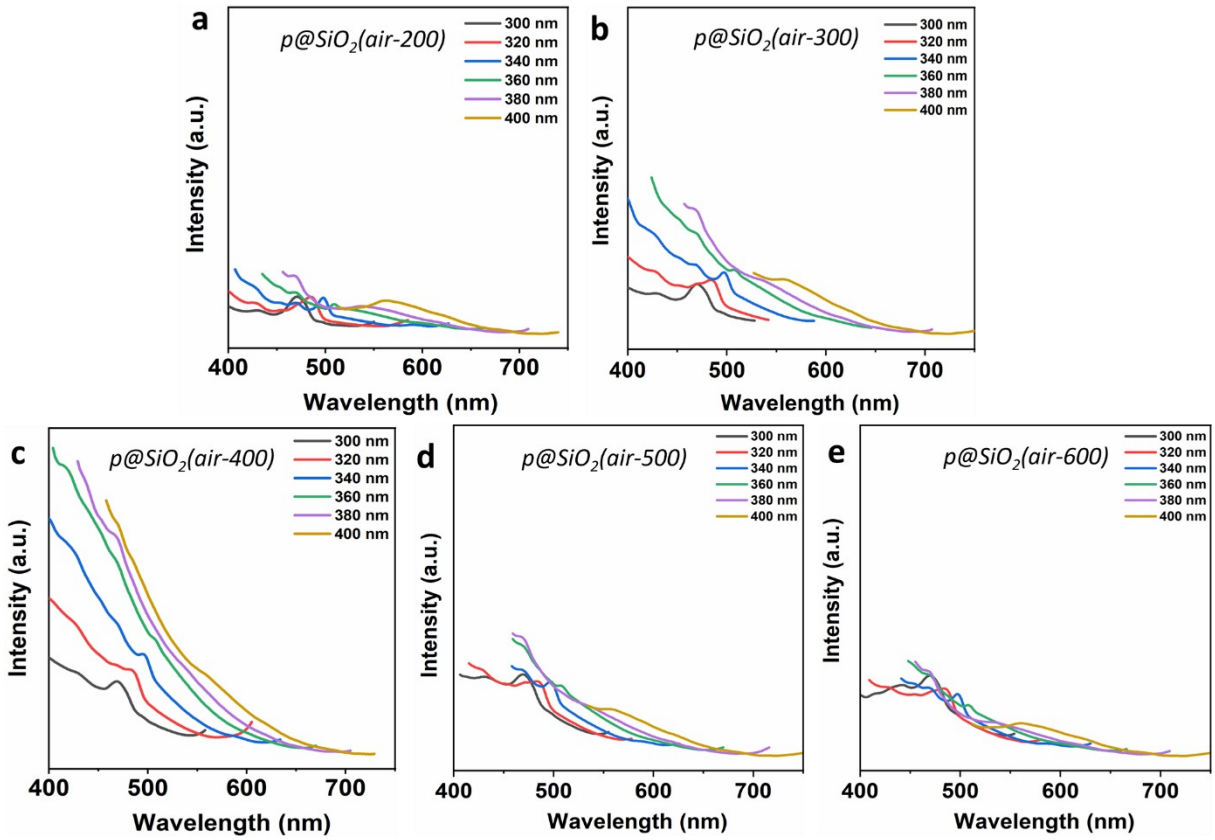

Fig. S12 FL spectra of annealed p@SiO_2 (in air at different temperatures) under different excitation wavelengths.

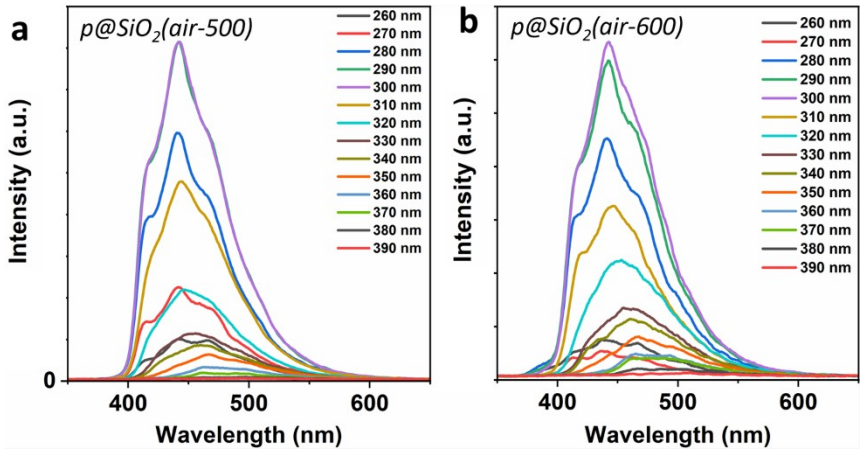

Fig. S13 Afterglow spectra of annealed p@SiO_2 (in air at different temperatures) under different excitation wavelengths.

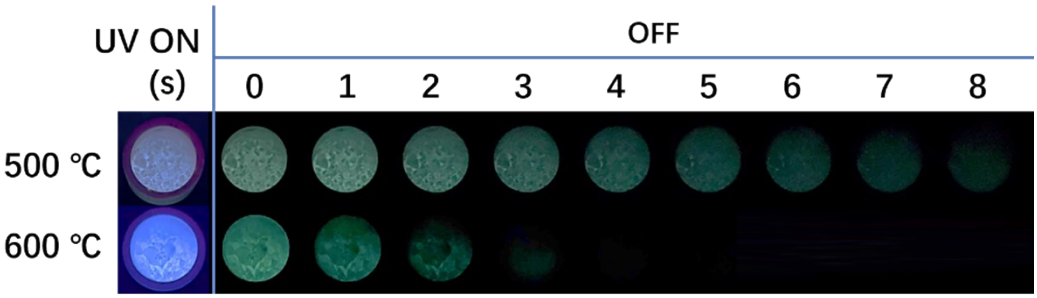

Fig. S14 Digital photos of annealed p@SiO_2 (in air at 500 and 600 °C) under 365 nm on/off stimuli.

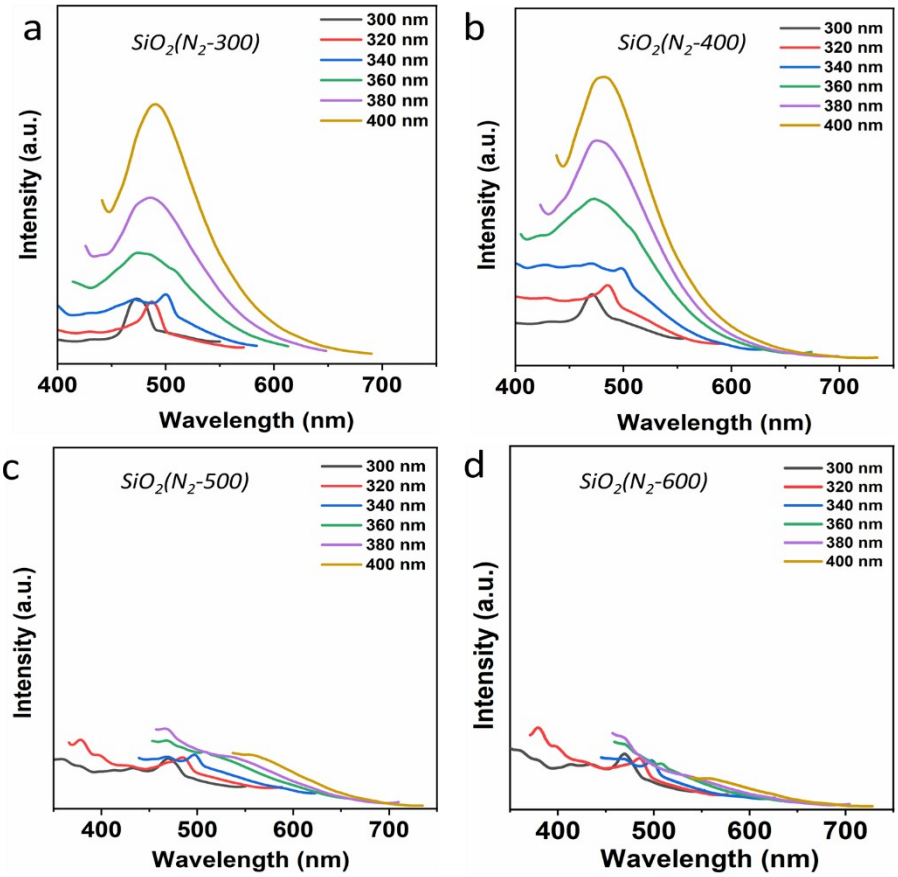

Fig. S15 FL spectra of annealed Stöber SiO_2 (in N_2 at different temperatures) under different excitation wavelengths.

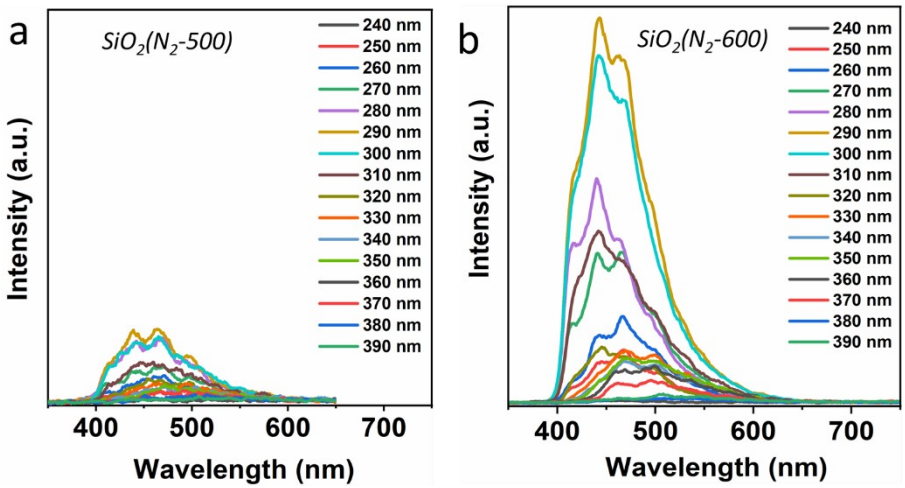

Fig. S16 Afterglow spectra of annealed Stöber SiO_2 (in N_2 at different temperatures) under different excitation wavelengths.

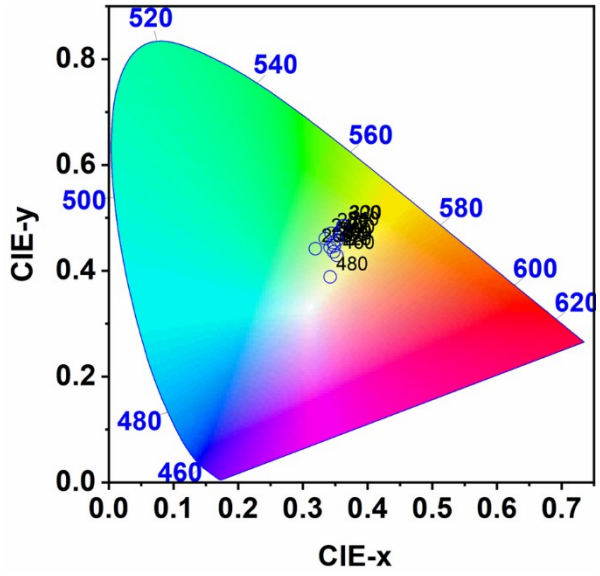

Fig. S17 CIE coordinates of afterglow emissions of ***D-5*** under different excitation wavelengths (*Ex.* 240 ~ 480 nm).

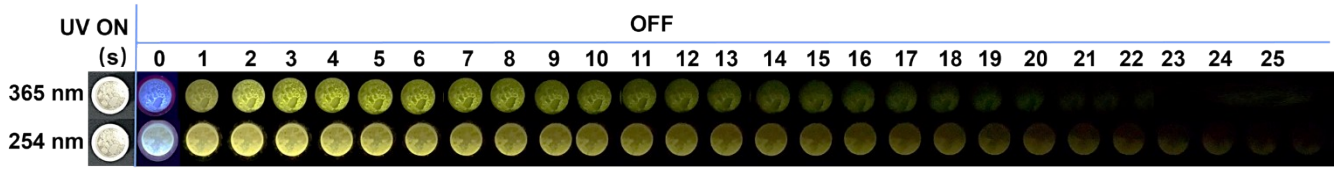

Fig. S18 Snapshots of FL and afterglow emission of ***D-5*** under 365 nm and 254 nm excitation.

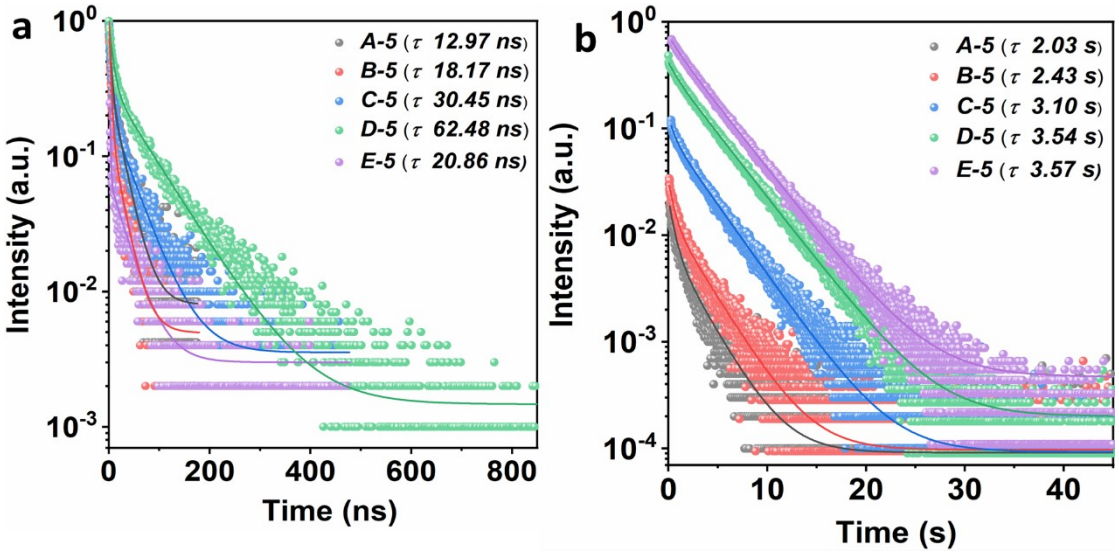

Fig. S19 Time-resolved (a) FL spectra of ***A-5*** ~ ***E-5*** (*Ex.* 320 nm, *Em.* 493 nm) and (b) afterglow decay spectra of ***A-5*** ~ ***E-5*** (*Ex.* 320 nm, *Em.* 571 nm).

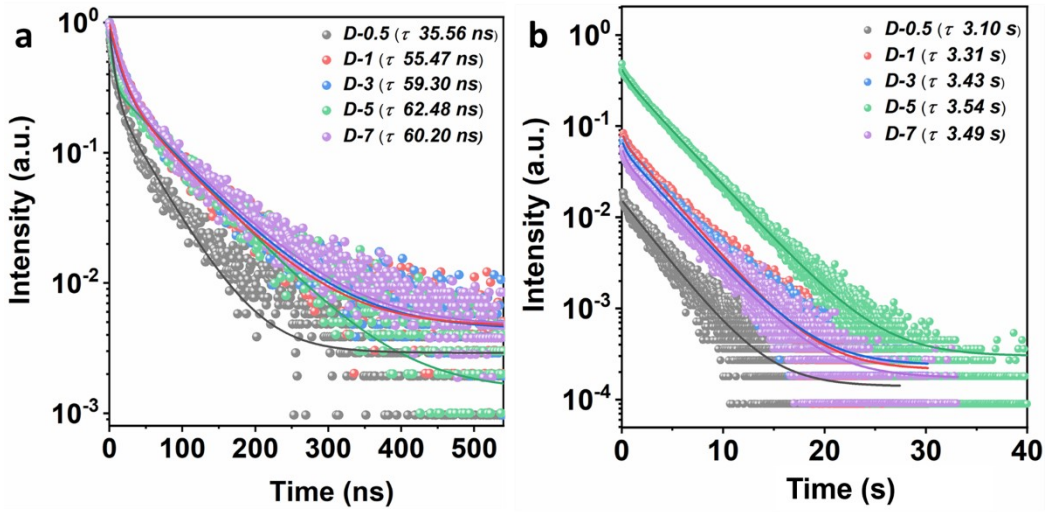

Fig. S20 Time-resolved (a) FL spectra of ***D-0.5*** ~ ***D-7***(*Ex.* 320 nm, *Em.* 493 nm) and (b) afterglow decay spectra of ***D-0.5*** ~ ***D-7*** (*Ex.* 320 nm, *Em.* 571 nm).

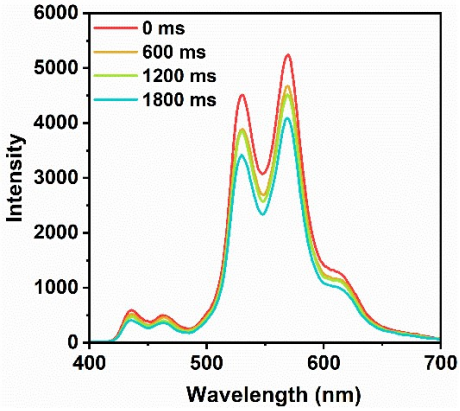

Fig. S21 Afterglow profiles of ***D-5*** at different delayed times.

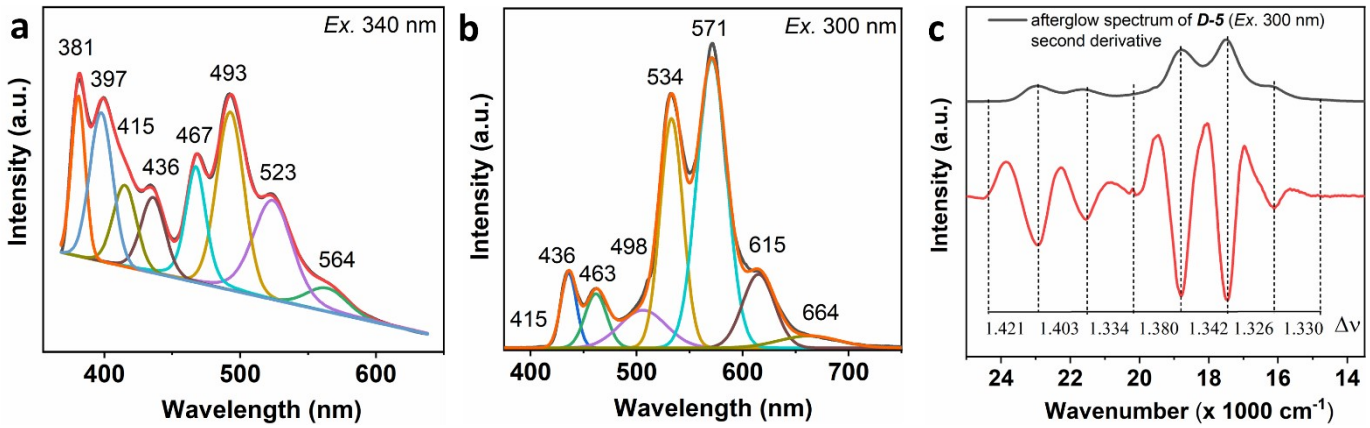

Fig. S22 Gaussian fitting of (a) FL (*Ex.* 340 nm) and (b) afterglow spectrum (*Ex.* 320 nm) of ***D-5*** and (c) the corresponding second derivative.

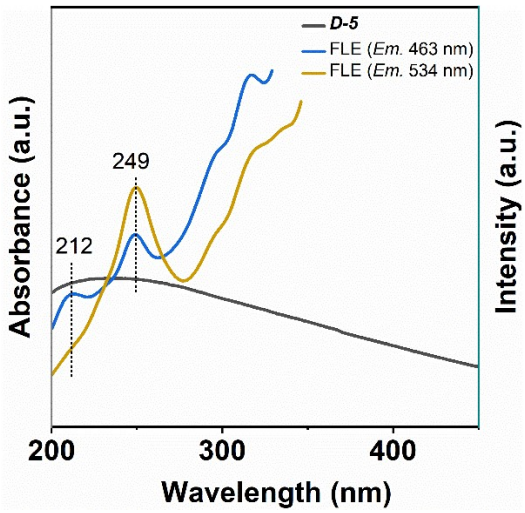

Fig. S23 Absorbance and fluorescence excitation spectra of ***D-5***.

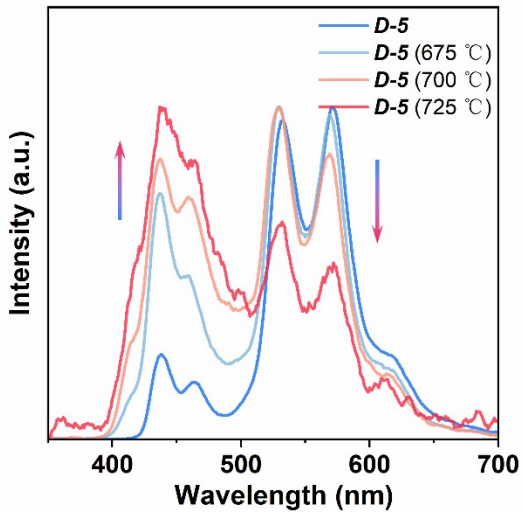

Fig. S24 Afterglow spectra (*Ex.* 320 nm) of ***D-5*** after further air-annealing treatment at different temperatures (675, 700, and 725 °C) for 4 h.

3.3 Application demonstration

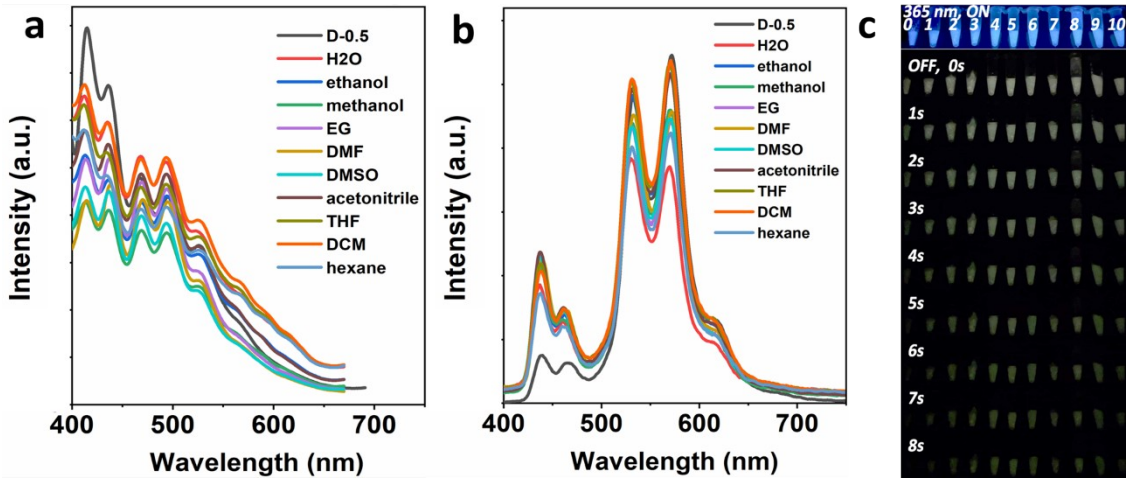

Fig. S25 (a) Fluorescence spectra and (b) afterglow spectra of ***D-0.5*** socked in different solvents, and (c) the corresponding digital photos under 365 nm UV light ON/OFF irradiation.

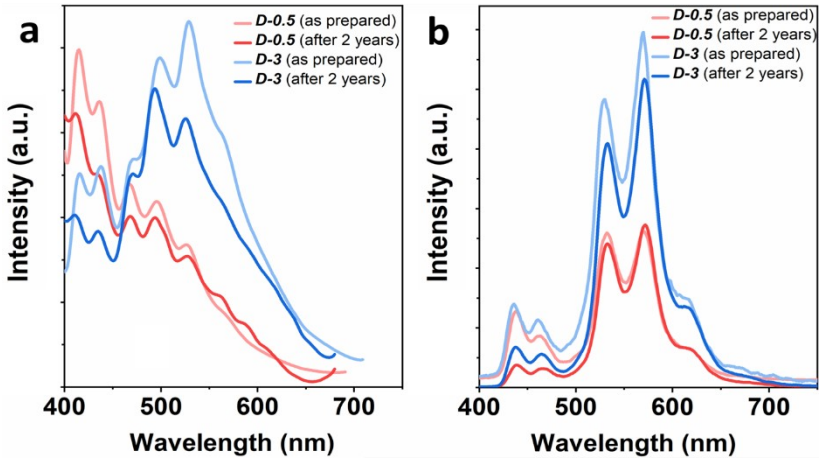

Fig. S26 (a) FL and (b) afterglow spectra of ***D-0.5*** and ***D-3*** as prepared and stored after two years.

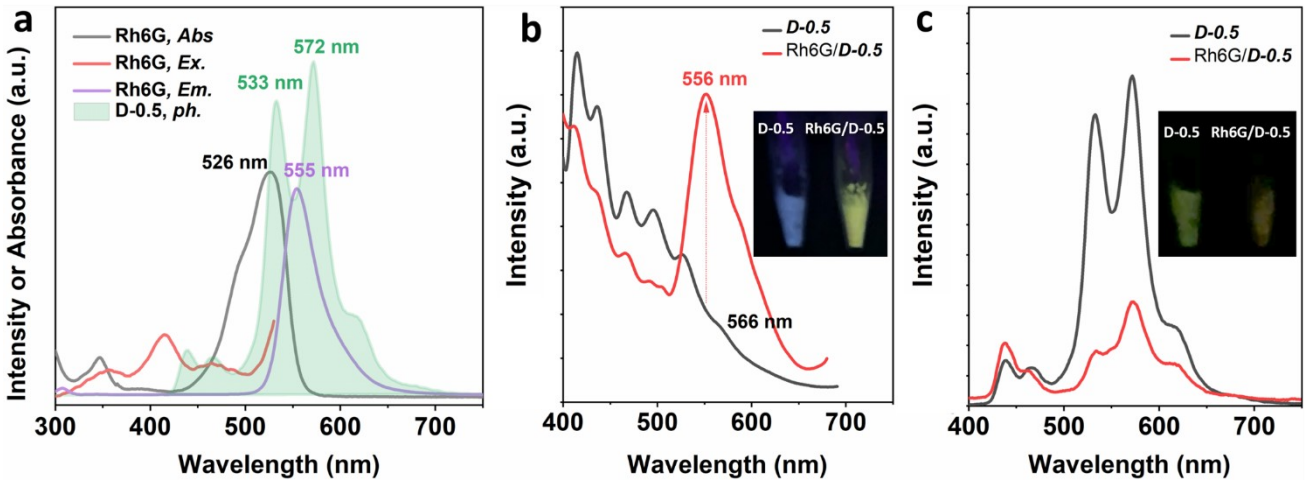

Fig. S27 (a) Absorbance spectrum and fluorescence excitation/emission spectra of Rh6G, and afterglow spectrum of ***D-0.5***, (b) fluorescence and (c) afterglow spectra of ***D-0.5*** and Rh6G/***D-0.5*** hybrids, and inserts are the corresponding digital photos.

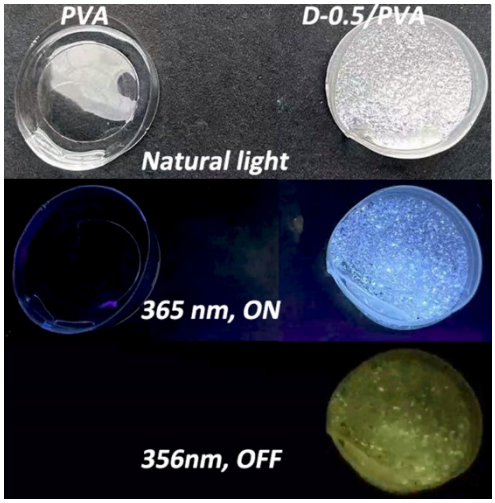

Fig. S28 Digital photos of pure PVA film and ***D-0.5***/PVA hybrid films under natural light, 365 nm UV light ON/OFF irradiation.

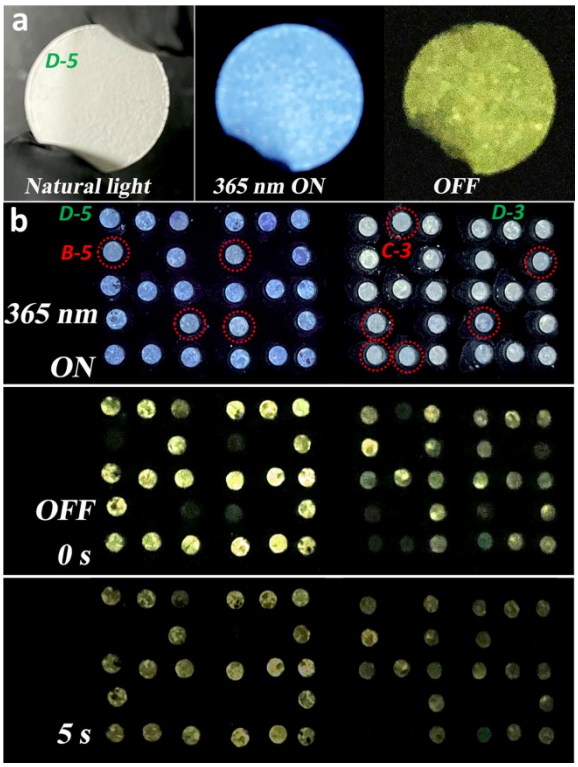

Fig. S29 (a) Images of mechanical-pressed PVA tablets containing 10 wt% of ***D-5*** under natural light and 365 nm UV irradiation on/off. (b) Code information composed of diverse doped silica under 365 nm UV irradiation on/off with time.

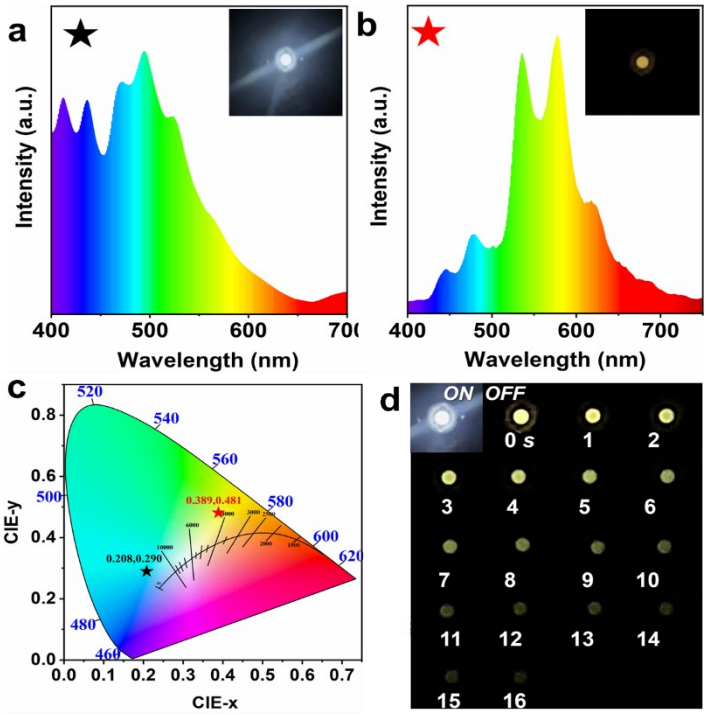

Fig. S30 (a) FL and (b) afterglow spectra of ***D-5***-coated LED device and inserts the LED light photos, and (c) CIE coordinates of FL and afterglow emission. (d) UV-on/off triggered LED light of ***D-5***.

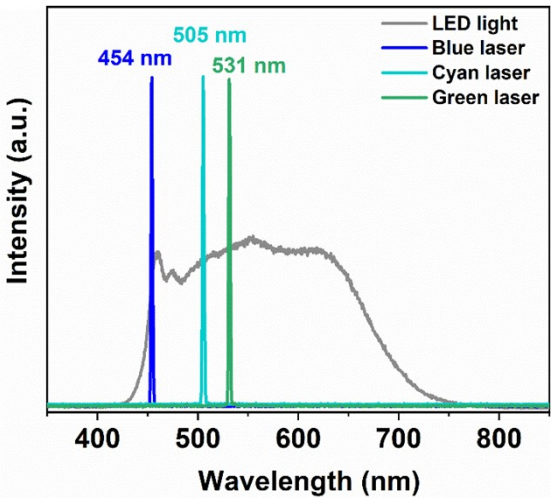

Fig. S31 Wavelength ranges of available light sources.

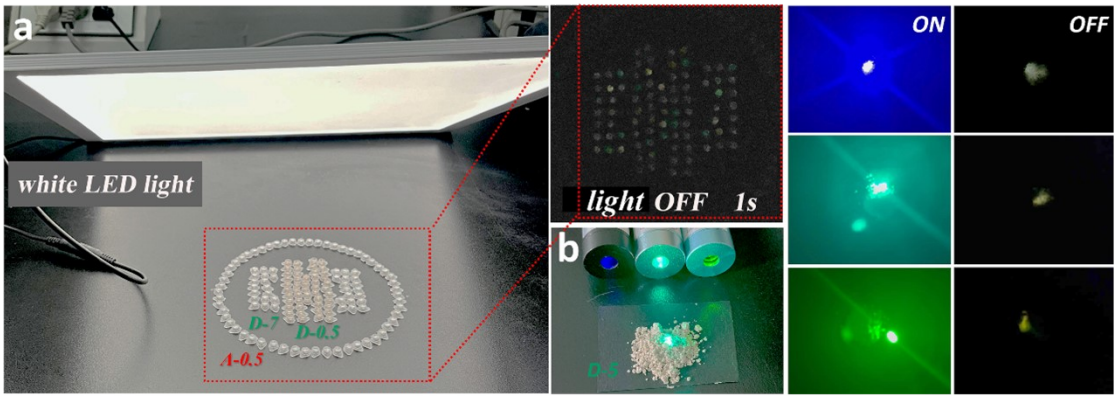

Fig. S32 (a) White shadowless lamp-triggered afterglow emission of the pattern composed of ***A-0.5***, ***D-5***, and ***D-7***. (b) Afterglow emission of ***D-5*** powder triggered by common laser pointers.

With the outstanding stability and distinctive photoluminescence characteristics of the doped silica, we demonstrated their preliminary applications as secondary excitation sources, in afterglow film, and in multi-level information encryption (Figure S27 ~ S32). Due to the large spectral-overlapping integrals between the afterglow emission of ***D-0.5*** and the excitation spectra of rhodamine 6G (Rh6G) (Figure S27a), ***D-0.5*** can potentially serve as a secondary excitation source to activate the FL of Rh6G after ceasing excitation. Powder mixture charged with ***D-0.5*** and Rh6G exhibited yellow FL emission under 365 nm of UV light, and an orange afterglow appeared when ceasing excitation (Figures S27b, c). In contrast, ***D-0.5*** powder exhibited its intrinsic blue FL and yellow afterglow. Leveraging the hydrophilicity, the doped silica can be well dispersed in a polyvinyl alcohol (PVA) solution to formulate an encrypted security ink. A PVA film incorporated ***D-0.5*** still exhibited blue FL and yellow afterglow emission under 365 nm excitation (Figure S28). Similarly, the powder mixture of PVA and doped silica can be easily mechanically pressed into PVA tablets, of which the intrinsic photoluminescence properties of the doped silica were preserved (Figure S29a).

As such, we demonstrated a promising application of the doped silica as innovative materials for multistate anti-counterfeiting and multistage information encryption. Four PVA tablets charged with doped silica (***B-5***, ***D-5***, ***C-3***, and ***D-3***) were encrypted into a pattern "8888" (Figure S29b). Under 365 nm excitation, two parts of the pattern "8888" exhibited blue (left) and white-blue (right) colors; once ceasing excitation ceased, the pattern suddenly changed to yellow "2345" with more than 5 s of lasting time. The PVA hybrid films and tablets retained their photoluminescence properties without degradation for more than one year under ambient storage conditions, highlighting the engineering property and practical applicability. We also demonstrated an afterglow-emitting LED using the doped silica as yellow afterglow-emitting dopants in the emissive layer (Figure S30). Due to the high quantum yield and wide excitation, the afterglow properties of ***D-5*** can also be excited by common laser pointers and even a white shadowless lamp (Figures S31, S32).

4. Tables

Table S1. Photoluminescence properties (*Ex.* 365 nm) of annealed silica from initial p@SiO_2.

initial SiO_2	T (°C)	N_2			air		
		fluorescence	afterglow	delay time (s)	fluorescence	afterglow	delay time (s)
p@SiO_2	100	-	-	-	-	-	-
	200	-	-	-	dull-bule	-	-
	300	dull-bule	-	-	blue	-	-
	400	blue	-	-	blue	-	-
	500	blue	-	-	purple-blue	blue-green	8
	600	bluish-white	-	-	purple-blue	blue-green	3
	700	bluish-white	dull-yellow	2	-	-	-
	800	bluish-white	yellow	7	-	-	-
	850	blue	yellow	19	-	-	-
	900	purple-blue	yellow	17	-	-	-
Stöber SiO_2	300	blue-green	-	-	-	-	-
	400	blue-green	-	-	-	-	-
	500	blue-green	dull yellow-green	2	-	-	-
	600	dull-blue	dull yellow-green	5	-	-	-

Table S2. Photophysical parameters of doped silica at 300 K.

Doped silica	*Fluorescence*					*Afterglow*				
	$E_x./E_m.$ (nm)	τ_1 (ns)/[%]	τ_2 (ns)/[%]	τ_{Avg} (ns)	*QY* (%)	$E_x./E_m.$ (nm)	τ_1 (s)/[%]	τ_2 (s)/[%]	τ_{Avg} (s)	*QY* (%)
p@SiO₂ (air-500)		3.53/33.54	14.65/66.46	10.92	-	320/493	0.32/29.15	1.84/71.85	1.42	-
A-5		3.58/46.75	21.22/53.25	12.97	3.70	320/493	0.27/25.36	1.28/74.64	1.02	-
						320/571	0.57/27.67	2.60/72.33	2.03	1.77
B-5		3.98/22.96	22.40/77.04	18.17	3.91	320/493	0.29/30.01	1.47/69.99	1.16	-
						320/571	0.52/18.29	2.85/81.71	2.43	2.66
C-5	320/493	4.60/29.92	41.48/70.08	30.45	8.67		0.58/7.57	3.30/92.43	3.10	6.35
E-5		1.30/38.92	33.31/61.08	20.86	8.39		1.12/4.90	3.57/95.11	3.45	14.05
D-0.5		6.38/24.75	45.16/75.25	35.56	-		3.39/32.60	2.96/67.40	3.10	-
D-1		13.22/27.77	71.71/72.23	55.47	-	320/571	0.27/2.19	3.37/97.81	3.31	-
D-3		13.11/25.75	75.32/74.25	59.30	-		0.36/2.78	3.52/97.22	3.43	-
D-7		13.50/26.61	77.13/73.39	60.20	-		0.39/3.34	3.60/96.66	3.49	-
D-5	320/381	29.04/33.55	112.21/66.45	84.30	-	320/415	0.04/91.56	0.68/8.44	0.09	-
	320/397	13.36/18.72	84.91/81.28	71.51	-	320/435	2.58/55.87	2.58/44.13	2.58	-
	320/415	11.01/21.99	73.75/78.11	59.95	-	320/463	0.28/7.70	2.19/92.30	2.05	-
	320/436	10.05/14.98	61.19/85.02	53.53	-	320/498	2.45/56.13	2.45/43.87	2.45	-
	320/467	7.07/14.69	59.45/85.31	51.75	-	320/534	0.38/0.62	3.51/99.38	3.50	-
	320/493	**8.40/17.56**	**73.99/82.44**	**62.48**	**17.74**	**320/571**	**0.79/3.87**	**3.65/96.13**	**3.54**	**16.68**
	320/523	8.90/25.16	73.52/74.84	57.26	-	320/615	0.21/10.15	3.10/89.85	2.81	-
	320/564	9.32/36.11	70.16/63.89	48.19	-	320/664	0.07/4.81	2.48/95.19	2.39	-

	-	-	-	-	-	260/571	0.84/22.84	2.89/77.1	2.42	-
	-	-	-	-	-	360/571	0.03/2.93	2.82/97.07	2.74	-
	-	-	-	-	-	400/571	0.17/15.03	1.84/84.97	1.59	-

Table S3. Comparison of the afterglow lifetimes and quantum yields by various materials.

No.	Materials	Afterglow	E_x/E_m.	τ_{Avg} (s)	*QY%*	*Ref.*
1	**Phenol-doped SiO_2**	**-**	**320/571**	**3.54**	**16.68**	**This work**
2	o-CDs@CA	TADF, RTP	365/550 (TADF) 365/690 (RTP)	0.22 (TADF) 0.013 (RTP)	8.95 (TADF) 7.47 (RTP)	*10*
3	CDs@SiO_2	RTP	365/510	1.50	24.30	*11*
4	CDs@SiO_2	TADF, RTP	365/450 (TADF) 365/520 (RTP)	0.80 (TADF) 1.07 (RTP)	10.8 (TADF) 14.3 (RTP)	*12*
5	a-CDs/BA	RTP	350/530	1.6	8.7	*13*
6	URTP CDs	RTP	340/535	1.4	-	*14*
7	IbCzA-0.1%-PVA	TADF, UOP	330/395	1.81 (TADF) 1.76 (UOP)	19.8	*15*
8	CD@SNP (3)	RTP	365/400-550	2.17	13.8	*16*
9	Amine-doped SiO_2	TADF, RTP	320/435 (TADF) 320/564 (RTP)	4.06 (TADF) 1.51 (RTP)	7.47	*17*
10	C-bSNPs	RTP	270/480	3.8	26.51	*18*

Table S4. Photophysical parameters of ***D-5*** at different temperatures.

Temperature (°C)	*Afterglow*			
	E_x/E_m. (nm)	τ_1 (s)/[%]	τ_2 (s)/[%]	τ_{Avg} (s)
-170	320/436	0.13/19.76	1.13/80.24	0.93
-120		0.14/9.42	1.41/90.58	1.29
-70		0.18/9.44	1.73/90.56	1.59
-20		1.85/64.90	1.85/35.10	1.85
30		2.58/55.87	2.58/44.13	2.58
-170	320/571	2.85/18.89	4.44/81.11	4.14
-120		1.96/10.74	4.35/89.26	4.10
-70		1.37/2.83	4.05/97.17	3.97
-20		1.89/5.00	3.87/95.00	3.77
30		**0.79/3.87**	**3.65/96.13**	**3.54**

Table S5. Reported PL bands of defects in amorphous SiO_2.

Emission wavelength (nm)	Defect	Structural model	References
370, 390, 415, 435	oxygen deficient center (ODC)	dioxasilyrane [=Si(O_2)] + silylene [=Si:] pairs 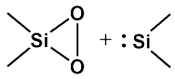 twofold coordinated silicon lone pair	19-22
413		centers O-Si-O	21, 22
459	neutral oxygen vacancy (NOV)	≡Si–Si≡	19-22
525, 564, 590	E'-center	≡Si·, $^{+}$Si≡, or ≡SiH	22-24
564	nonstoichiometric SiO_x	SiO_x, 1 < x < 2	23
652-689	nonbridging oxygen hole center (NBOHC)	≡Si-O·	20, 22, 23, 25
408, 422, 460, 484, 520, 564, 620, 680	carbon substitutional defect of silica (carbon impurity)	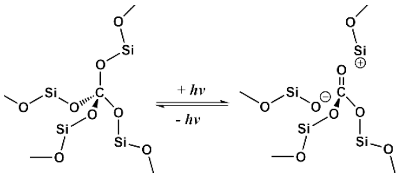	26, 27

References

1 W. Stöber, A. Fink and E. Bohn, Controlled growth of monodisperse silica spheres in the micron size range, *J. Colloid Interface Sci.,* 1968, **26**, 62.

2 Y. Sun, J. Liu, X. Pang, X. Zhang, J. Zhuang, H. Zhang, C. Hu, M. Zheng, B. Lei and Y. Liu, Temperature-responsive conversion of thermally activated delayed fluorescence and room-temperature phosphorescence of carbon dots in silica, *J. Mater. Chem. C,* 2020, **8**, 5744.

3 Y. Luo, Q. Jiang, J. Liu, H. Yang, X. Liao, F. Huang, J. Zhuang, C. Hu, B. Lei, Y. Liu and J. He, Mesoporous collapsing encapsulated carbon dots: Direct evidence for the effect of multiple-confined interactions of silica on efficient long-lived phosphorescence, *Chem. Eng. J.,* 2024, **486***,* 150436.

4 K. Jiang, X. Gao, X. Feng, Y. Wang, Z. Li and H. Lin, Carbon Dots with Dual-Emissive, Robust, and Aggregation-Induced Room-Temperature Phosphorescence Characteristics, *Angew. Chem. Int.,* 2020, **59**, 1263.

5 J. Liu, N. Wang, Y. Yu, Y. Yan, H. Zhang, J. Li and J. Yu, Carbon dots in zeolites: A new class of thermally activated delayed fluorescence materials with ultralong lifetimes, *Sci. Adv.,* 2017, **3**, 1603171.

6 H. Uoyama, K. Goushi, K. Shizu, H. Nomura and C. Adachi, Highly efficient organic light-emitting diodes from delayed fluorescence, *Nature,* 2012, **492**, 234.

7 J. Yoo, S. Han, W. Park, T. Lee, Y. Park, H. Chang, S. K. Hahn and W. Kwon, Defect-Induced Fluorescence of Silica Nanoparticles for Bioimaging Applications, *ACS Appl. Mater. Interfaces,* 2018, **10**, 44247.

8 Y. Deng, D. Zhao, X. Chen, F. Wang, H. Song and D. Shen, Long lifetime pure organic phosphorescence based on water soluble carbon dots, *Chem. Commun.,* 2013, **49***,* 5751.

9 P. Jiang, B. Ding, J. Yao, L. Zhou, Z. He, Z. Huang, C. Yin, H. Tian and X. Ma, Thermal Modulation of Exciton Recombination for High-Temperature Ultra-Long Afterglow, *Angew. Chem. Int. Ed.,* 2025, **64***,* 202421036.

10 Y. Wang, K. Jiang, J. Du, L. Zheng, Y. Li, Z. Li, H. Lin, Green and Near-Infrared Dual-Mode Afterglow of Carbon Dots and Their Applications for Confidential Information Readout, *Nano-Micro Lett*. 2021, **13**, 198.

11 Y. Sun, S. Liu, L. Sun, S. Wu, G. Hu, X. Pang, A. Smith, C. Hu, S. Zeng, W. Wang, Y. Liu, M. Zheng, Ultralong lifetime and efficient room temperature phosphorescent carbon dots through multi-confinement structure design. *Nat. Commun*. 2020, **11**, 5591.

12 Y. Sun, J. Liu, X. Pang, X. Zhang, J. Zhuang, H. Zhang, C. Hu, M. Zheng, B. Lei, Y. Liu, Temperature-responsive conversion of thermally activated delayed fluorescence and room-temperature phosphorescence of carbon dots in silica, *J. Mater. Chem. C* 2020, **8**, 5744.

13 W. Li, W. Zhou, Z. Zhou, H. Zhang, X. Zhang, J. Zhuang, Y. Liu, B. Lei, C. Hu, A universal strategy for activating multi-color room temperature afterglow of carbon dots in boric acid matrix, *Angew. Chem. Int. Ed.* 2019, **131**, 7356.

14 K. Jiang, Y. Wang, X. Gao, C. Cai, H. Lin, Facile, quick, and gram-scale synthesis of ultralong room temperature phosphorescent carbon dots by microwave irradiation, *Angew. Chem. Int. Ed*. 2018, **57**, 6216.

15 Y. Yang, Y. Liang, Y. Zheng, J.-A. Li, S. Wu, H. Zhang, T. Huang, S. Luo, C. Liu, G. Shi, F. Sun, Z. Chi, B. Xu, Efficient and Color-Tunable Dual-Mode Afterglow from Large-Area and Flexible Polymer-Based Transparent Films for Anti-Counterfeiting and Information Encryption, *Angew. Chem. Int. Ed.* 2022, **61**, e202201820.

16 C. Han, S. H. Lee, K. Lee, H. Chang, H. Jo, S. Seo, H. Park, S. K. Hahn, Y. H. Kim, W. Kwon, Long-Lived Room-Temperature Phosphorescence from Silica Nanoparticles with In Situ Generated Carbonaceous Defects for Blue Organic Light-Emitting Diodes, *ACS Appl. Mater. Interfaces* 2024, **16**, 65012.

17 Y. Sun, X. Shao, L. Sui, Y. Yang, Y. Zhong, S. Yang, J. Liu, Multi-defects within silica inducing coexistence of thermal activated delayed fluorescence and room temperature phosphorescence, *Chem. Eng. J*. 2025, **519**, 164772.

18 H. Chang, Y. Park, K. Kim, C. Han, Y. Yoon, W. Yoo, J. Yoo, D. Lee, H. Han, K. Kim, J. Joo, W. Kwon, Room-temperature phosphorescence of defect-engineered silica nanoparticles for high-contrast afterglow bioimaging, *Chem. Eng. J.* 2024, **493**,

152529

19 T. Uchino, N. Kurumoto and N. Sagawa, Structure and formation mechanism of blue-light-emitting centers in silicon and silica-based nanostructured materials, *Phys. Rev. B,* 2006, **73**, 233203.

20 H. Nishikawa, T. Shiroyama, R. Nakamura, Y. Ohki, K. Nagasawa and Y. Hama, Photoluminescence from defect centers in high-purity silica glasses observed under 7.9-eV excitation, *Phys. Rev. B,* 1992, **45**, 586.

21 D. P. Yu, Q. L. Hang, Y. Ding, H. Z. Zhang, Z. G. Bai, J. J. Wang, Y. H. Zou, W. Qian, G. C. Xiong and S. Q. Feng, Amorphous silica nanowires: Intensive blue light emitters, *Appl. Phys. Lett.,* 1998, **21**, 3076.

22 C. F. Sánchez, J. A. RodrÍguez and C. DomÍnguez, Synthesis of sol-gel SiO_2-based materials using alkoxydisilane precursors: mechanisms and luminescence studies, *J Sol-Gel Sci. Technol.,* 2015, **73**, 417.

23 I. I. Hinić, G. M. Stanišić and Z. V. Popović, Influence of the synthesis conditions on the photoluminescence of silica gels, *J. Serb. Chem. Soc.,* 2003, **12**, 953.

24 D. G. Yuri, S. H. Lin and Y. T. Chen, The photoluminescence from hydrogen-related species in composites of nanoparticles, *Appl. Phys. Lett.,* 1999, **6**, 778.

25 M. Cannas and F. M. Gelardi, Vacuum ultraviolet excitation of the 1.9-eV emission band related to nonbridging oxygen hole centers in silica, *Phys. Rev. B,* 2004, **69**, 153201.

26 W. H. Green, K. P. Le, J. Grey, T. Au and M. J. Sailor, White Phosphors from a Silicate-Carboxylate Sol-Gel Precursor That Lack Metal Activator Ions, *Science,* 1997, **5320**, 1826.

27 H. Chang, Y. Park, Y. Kim, C. Han, Y. Yoon, W. Yoo, J. Yoo, D. Lee, H. Han, K. Kim, J. Joo and W. Kwon, Room-temperature phosphorescence of defect-engineered silica nanoparticles for high-contrast afterglow bioimaging, *Chem. Eng. J.*, 2024, **493**, 152529.